RSC Advances

ROYAL SOCIETY OF CHEMISTRY

www.rsc.org/advances

RSC Advances

ARTICLE

Sustainable Synthesis of Highly Efficient Sunlight-driven Ag Embedded AgCl Photocatalyst

Received 00th January 20xx,
Accepted 00th January 20xx

DOI: 10.1039/x0xx00000x

www.rsc.org/

Z. Shen[a, ‡], B. Liu[b, ‡], V. Pareek[a], S. Wang[a], X. Li[b], L. Liu[a,*], S. Liu[a]

Plasmonic silver embedded silver chloride (Ag@AgCl) nano-photocatalysts were synthesized in a microbe-free aqueous Lysogeny broth (Miller) solution, at room temperature with 5 min sunlight exposure. The nanohybrids were formed by *in situ* photoreduction and photo-accelerated ripening of AgCl colloids, promoted by the attached biomolecular ligands. Compared with commercial TiO_2, the biogenic Ag@AgCl nanocomposites demonstrate higher photocatalytic activity towards decomposition of organic dye solution under solar light with excellent photocatalytic stability.

Introduction

Most previously discovered photocatalysts (*i.e.* TiO_2, ZnO) require ultraviolet (UV) light activation due to their wide band gaps, thus only 4% of sunlight can be utilized. Benefiting from the surface plasmon resonance (SPR) of noble metals, hybrid nanostructured semiconductors such as Au@TiO_2[1] and Ag@ZnO [2-3] have light-absorption extended to visible light range. Other plasmonic photochtalysts, including Ag@AgX (X = Cl, Br, I) analogous nanocomposites, are expected to play important roles in solar energy conversion and environmental remediation as well.[4-5] Since Wang and co-workers reported visible light driven decomposition of methyl orange (MO) by Ag@AgCl, intensive studies have been devoted to the pollutants degradation.[6-7] Ag@AgX also shows promising performance in killing waterborne microbial pathogens.[8-9] Recently, An et al. developed shaped AgX:Ag (X = Cl, Br) for reduction of CO_2 to methanol.[10]

In general, there are two main research directions to enhance the photocatalytic activity of Ag@AgX. One is to manipulate the shape of the catalysts.[11] Among them, cube based Ag@AgCl has been well explored to efficiently decompose organic dyes.[12-15] In most cases, multiple steps or external stabilizer like polyvinyl pyrrolidone (PVP) are required to control the fast precipitation of AgCl thereby hampering the prospects for practical applications. Secondly, since the photocatalytic activity is strongly dependent on the size, tremendous endeavours in terms of reducing the dimension of Ag@AgCl from micrometre to ~ 100 nm have been carried out.[16] Moreover, in the context of the current drive to conserve resources and protect the environment, facile phytosynthesis using beet and sugar cane juice has been attempted recently.[17-18] Nevertheless, the protocols still required high temperature (80-100 °C) and high pressure (1930 kPa). Accordingly, there is a need for an environmentally benign process for Ag@AgCl preparation which occurs at ambient temperatures. As biogenic technology using bacteria or other microorganisms usually occur at ambient pressure and temperature, it might have a lower environmental impact.[19] Jiang and co-workers have demonstrated that *Gluconacetobacter xylinum* enabled fabrication of antimicrobial Ag@AgCl composite.[20] The *G. xylinum* was cultured in broth at 30 °C for 5 days followed by $AgNO_3$ challenge for 2 to 3 days to obtain Ag/AgCl nanoparticles. At last, the solution containing Ag/AgCl particles and cells was filtered through membrane to remove bacterial cell bodies. Apparently, there are disadvantages in the use of microbes, e.g., time consuming in microbe culture[21] and downstream purification. Thus, the importance of cell-free biosystems with higher product yields and faster reaction rates has been acknowledged.[22]

Our previous microbe-free strategy proves that various nano/micro particles with controlled morphology and size could be obtained in microbial culture broths alone.[23] Specifically, microbe-independent colloidal AgCl formation was observed in tryptic soy broth (TSB) and Lysogeny broth (LB).[24] LB contains yeast extract and peptone that are rich in amino acids and peptides. Inspired by the latest results on the electron transfer (ET) peptide mediated Ag nanoparticle (NP) formation by laser irradiation on AgCl,[25] we hypothesize that the biogenic AgCl might be partially reduced under sunlight to get small plasmonic Ag@AgCl. Additionally, an in-situ

[a] Department of Chemical Engineering, Curtin University, GPO Box U1987, Perth, Western Australia 6845, Australia.
[b] School of Environmental Science and Technology, Dalian University of Technology, Dalian 116024, China

Electronic Supplementary Information (ESI) available: Effect of broth component and solar light irradiation time on the synthesis and performance of 1Ag@AgCl samples; UV-vis spectra of 40AgNaCl5m, 40Ag(NaCl+YE)5m and 40AgLB5m; UV-vis spectra of 40AgLB5m etched by NH_4OH and HNO_3, respectively; Table S1 summarizes the degradation percentage of 10 ppm MB pollutant in the presence of various 1Ag samples under solar light for 60 min; DLS Z-average particle size of Ag@AgCl spheres prepared with different [Ag^+] concentration. See DOI: 10.1039/x0xx00000x

photoreduction strategy is expected to introduce midgap defect states in AgCl to enhance photocatalytic activities.[26] In this study, stable AgCl colloidal spheres with a size of ~ 50 nm were formed first through a precipitation reaction of $AgNO_3$ and NaCl in LB Miller broth. By rationally changing the precursor concentration and light exposure time, we could finely tune the bandgap of the composites. After 5 min solar light activation at room temperature, the as-synthesized Ag@AgCl particles demonstrate better performance than commercially available P25 (TiO_2) in the degradation of Rhodamine 6G. The excellent activities could be attributed to the embedded Ag NPs associated with stronger plasmon resonance of Ag@AgCl composites. Herein, we for the first time develop a facile one-pot biological process that is superior to most conventional biomimetic methods in preparing Ag@AgCl NPs with unique configuration.

Results and discussion

Broth and light-dependent Ag@AgCl nanoparticle formation

We screened the broths for Ag@AgCl formation using a variety of microbial culture medium including Lysogeny broth (LB), Nutrient broth (NB), tryptic soy broth (TSB), and yeast mold broth (YMB). As reported in our previous study, after mixing 2 mM $AgNO_3$ with equal volume of original broths under ambient light at room temperature for 15 days, silver nanoparticles were mainly formed in NB and YMB broths; while Ag nanoparticle decorated silver chloride (Ag@AgCl) was the major product in LB and TSB. This is due to the presence of high concentration of NaCl.[24]

From the viewpoint of renewable energy utilization, sunlight is the most attractive candidate for nanomaterial manufacture. Therefore we performed the same reactions using a sunlight simulator and found particle formation rate was increased significantly compared with that under ambient light.

It can be seen in Figure S1A that in just 5 min, 1AgLB5m (X-Ag-Y-Z, where X denotes the Ag^+ concentration in mM, Y is referred to the broth name and Z denotes the solar light irradiation time) sample displays a unique purplish colour of Ag@AgCl nanocomposites.[9, 27] Other three samples show yellow to brown colours of Ag NPs solution. This is in agreement with their UV-vis absorption spectra (Figure S1B). In contrast to other samples, 1AgLB5m has a much wider absorption band in the wavelength range of 320-900 nm and the absorbance increased over the entire region as the irradiation time increased from 30 seconds to 10 minutes (Figure S1C). This characteristic absorption is attributed to the surface plasmon resonance (SPR) of the *in situ* formed Ag NPs[28] and AgCl nanohybrid. Figure S1D shows XRD patterns of samples after 30 min under sunbeam. For all samples, the peaks at 38.2°, 44.2°, 64.6° and 76.6° correspond to the (111), (200), (220) and (311) planes of the cubic phase of Ag^0 (JCPDS file: 65-2871). Peaks at 27.7° and 32.1° are belonging to the (111) and (200) planes of the cubic phase of AgCl (JCPDS file: 31-1238).

We further evaluated the photocatalytic degradation of 10 ppm methylene blue (MB) over these samples. As shown in Table S1, under the same degradation conditions, 1AgYMB5m sample showed limited or no photocatalytic activity. 1AgLB5m showed the most pronounced activity and decomposed 61.6% MB after 60 min, while 1AgNB5m and 1AgTSB5m decomposed 46.5% and 41.8% MB, respectively. The photocatalytic activity of the Ag@AgCl nanohybrids prepared in different broths was in the following order: AgLB > AgNB > AgTSB > AgYMB. A reduced activity was observed among all samples subjected to longer sunbeam irradiation (15 and 30 min, respectively). All the above results indicate that Ag@AgCl catalysts should be prepared in LB solution with short solar light activation. LB broth is the most commonly used medium for *E.coli* cell culture and contains 0.5% yeast extract, 1.0% peptone and 1.0% sodium chloride (~ 170 mM). To test the influence of silver precursor concentration, [Cl^-] was fixed while [Ag^+] was increased from 2.0 to 80.0 mM in final LB solution.

Effect of $AgNO_3$ concentration on photocatalytic performance

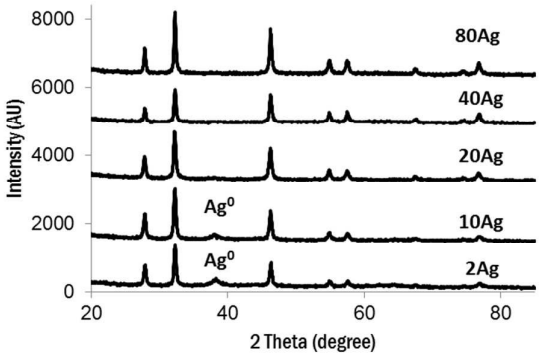

Fig. 1 XRD patterns of the XAgLB5m samples prepared from precursors with different [Ag^+] concentration (X refers to the final [Ag^+] concentration in mM).

Figure 1 presents the typical XRD patterns of Ag@AgCl nanocomposites with different silver precursor concentration. All samples clearly show diffraction peaks of AgCl. Though the photoreduction conditions are the same (5 min under simulated solar light), only 2AgLB5m and 10AgLB5m samples show diffraction peaks of metallic Ag at 38.2°. As [Ag^+] increased, the intensity of peaks at this position gradually decreased and no obvious peaks were observed in 40AgLB5m and 80AgLB5m samples. The possible reason is that the photo-reduced Ag NPs are small and might be buried inside the AgCl matrix as proposed in other studies.[13] Other characterization results in the following sections could verify the coexistence of Ag and AgCl phases.

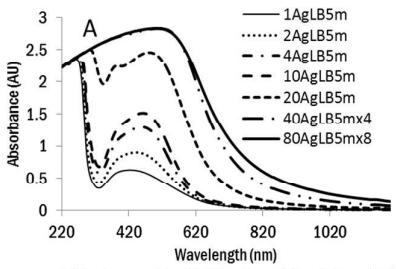

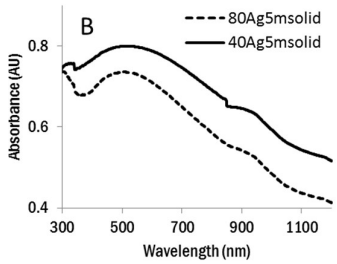

Fig. 2. (A) UV-vis absorption of XAgLB5m samples (X refers to the final [Ag^+] concentration in mM) in water. (B) UV-vis diffuse reflectance spectra of solid 40AgLB5m and 80 AgLB5m samples.

Most optical properties of Ag@AgCl were studied by the diffuse reflectance spectroscopy (DRS) of the nanohybrid powders.[29] However, the DRS requires large amount of samples and is not sensitive enough at detecting a small change in optical properties of materials, thus UV-vis absorption technique for kinetic study of Ag@AgCl formation was employed.[25, 30] As shown in Figure 2A, UV-vis absorption spectra are reliable for Ag@AgCl dispersions at low particle concentrations (up to 20AgLB5m sample; 40AgLB5m and 80AgLB5m samples need to be diluted further since a saturation plateau has been reached due to the high concentration of the nanoparticles. Moreover, noteworthy is that the mass ratio of Ag@AgCl in an 8-fold diluted 80AgLB5m and 4-fold diluted 40AgLB5m solution is 1.3 therefore a higher absorbance intensity was observed for 80AgLB5m8x sample.) All samples display strong absorption in both the UV and visible regions due to the characteristic absorption of the AgCl semiconductor and the SPR effect of the Ag nanocrystals. An increase in [Ag^+] concentration leads to a continued increment in the peak intensity. In visible region, the position of the maximum absorption wavelength (λ_{max}) was red-shifted from 425 to 520 nm. The huge shift is similar to the case of ripening of AgCl in ethylene glycol at 160 °C.[31] Dynamic light scattering (DLS) characterization (Table S2) and controlled etching experiments suggest that the red-shift is mainly induced by the size growth of AgCl colloids.[30] The UV-vis DRS of 40AgLB5m and 80AgLB5m are illustrated in Figure 2B. Again, three absorption bands at ~ 260, ~300 and ~ 520 nm could be ascribed to the large band gap of AgCl, tiny Ag clusters and relatively large Ag NPs embedded in AgCl matrix, respectively. The absorption intensity of 40AgLB5m is higher than that of 80AgLB5m from 300 to 1200 nm. According to the equation

$E_g = 1240/\lambda_g$ (eV) (1)

their indirect band gaps (E_g) were calculated to be 0.97 eV and 1.08 eV, respectively (Figure S4). The value of E_g is found to decrease dramatically after Ag doping. Since high doping densities cause the bandgap to shrink and the optical absorption depends on the defect state, the decrease in the E_g in the present system may be due to increase in the density of defect.[32] A higher light absorption on 40AgLB5m sample was linked to a better photocatalytic activity, which will be discussed in the following sections.

The morphology of 40AgLB5m was observed by SEM. As shown in Figure 3A, Ag@AgCl particles are spherical with a diameter around 50 nm, which is consistent with our DLS results. Some silver nanoparticles were produced by the

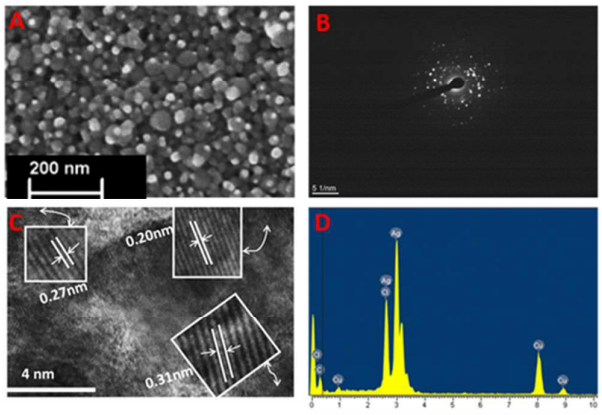

Fig. 3 SEM (A), SAED (B), HRTEM (C), and EDX (D) analysis of 40AgLB5m sample.

decomposition of AgCl under the high energy electron beam. In HRTEM image (Figure 3C), the lattice spacings of 0.31 and 0.27 nm are assigned to the (200) and (111) diffractions of AgCl.[33] The distinct lattice fringe of d = 0.20 nm matches with the crystallographic planes of Ag (200).[34] The SAED pattern shows a crystalline spot ring (Figure 3B), indicating the polycrystalline feature of the sample.[35] The chemical compositions of nanoparticles were analysed by EDX and XPS. The EDX spectrum (Figure 3D) shows peaks associated with Ag, Cl and several Cu peaks from TEM grid. The calculated atomic ratios of Ag to Cl in several spots were varied from 1.1 to 1.4, because of the sensitivity of AgCl to electron beam.

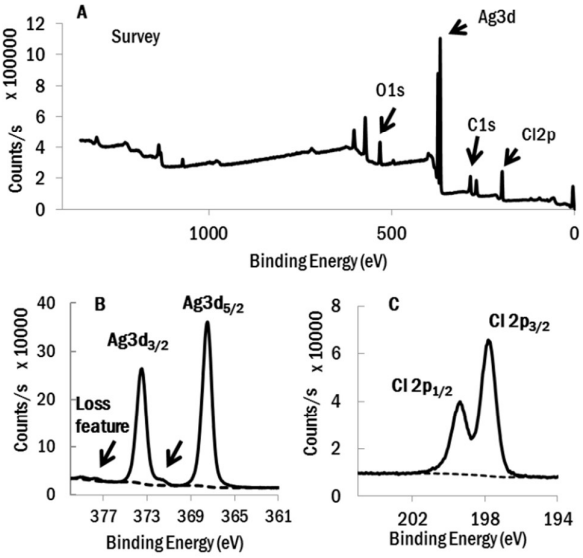

Fig. 4 XPS spectra of the 40AgLB5m: XPS survey spectrum (A), high resolution Ag3d spectrum (B), and high resolution Cl 2p spectrum (C).

XPS was employed to further investigate the composition of the as-prepared 40AgLB5m. Figure 4A shows the fully scanned XPS spectrum. The sample consists of Ag, Cl, O and C elements. In Figure 4C, the Cl 2p curve contains two peaks centred at 197.8 eV and 199.4 eV, attributed to the binding energies of Cl $2p_{3/2}$ and Cl $2p_{1/2}$, respectively. For high resolution Ag 3d spectra (Figure 4B), the peaks located at ~ 367.5 and 373.5 eV with a peak separation of 6.0 eV are ascribed to Ag $3d_{5/2}$ and Ag $3d_{3/2}$ binding energies, respectively. Compared with those of bulk Ag (Ag $3d_{5/2}$, 368.2 eV and Ag $3d_{3/2}$, 374.2 eV)[36], peak positions of Ag 3d shift remarkably to lower binding energies, which is mainly attributed to the higher valence of Ag in AgCl.[37] Moreover, loss features resulted from each spin-orbit component for metal Ag are also observed in Figure 4B.[38] These results corroborated with UV-vis investigations confirm the existence of Ag^0 in 40AgLB5m sample.

Identification of key components in LB broth for Ag@AgCl formation and possible biosynthesis mechanism

The aqueous solution of NaCl and yeast extract was mixed with Ag^+ individually to study their roles in Ag@AgCl formation. The UV-vis spectra recorded for all samples prepared under the same conditions was displayed in Figure S2. 40AgNaCl5m showed no absorption in the 250-900 nm regions, which confirms that without yeast extract (YE) and peptone involvement, AgCl could not readily be transformed to Ag@AgCl after 5 min solar light irradiation. 40AgYE only produced a typical Ag NPs single absorption band centred at *ca.* 460 nm. Notably, the position of major peak does not change at this wavelength (Figure S2B). In contrast, 40AgLB displayed typical Ag@AgCl absorption band as discussed before.

To understand the nanostructure of 40AgLB5m, control experiments with selective etching of AgCl and Ag NPs by aqueous solutions of NH_4OH and HNO_3 were performed as reported by Peng et al..[31] Figure S3A shows the UV-vis spectra of 40AgLB5m etched by different amounts of NH_4OH. We did not observe the SPR peak of Ag NPs when small amounts of NH_4OH reacted with the sample. Absorption peaks corresponding to free standing Ag NPs gradually emerged and blue-shifted when more (15-120 µL) NH_4OH is added. There is no obvious change in spectra of samples treated by excessive HNO_3 (Figure S3B). These results suggest that most Ag NPs could have resided deeply in AgCl colloids rather than attached to the particle surface, therefore, protected from HNO_3 attack. We initially thought our Ag@AgCl might follow the same mechanism by forming the bimodal AgCl first and then changing to uniform particles by dissolution of smaller nanoparticles and growth of the larger ones (Scheme 1A). However, original AgCl and final Ag@AgCl particles have the same diameter (data not shown). It is difficult to explain how Ag NPs were embedded into AgCl colloids unless we consider the fragmentation of AgCl under solar light irradiation.

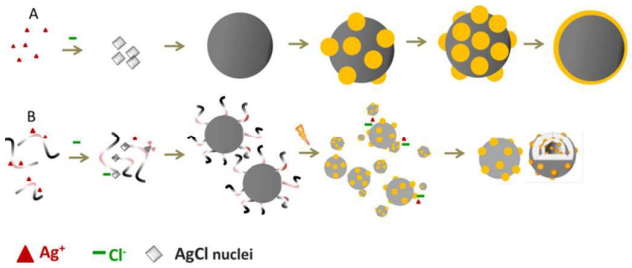

Scheme 1 Mechanisms proposed for biogenic Ag@AgCl formation through photo-induced and accelerated ripening process: (A) the growth of Ag@AgCl particles during a typical chemical reduction process, and (B) the formation of Ag@AgCl plasmonic nanohybrid within LB broth.

In the presence of DNA oligonucleotides, Wang et al. disclosed that remarkable fragmentation of AgCl particles occurred after UV irradiation for just 1.5 s.[39] More recently, electron transfer peptide has been reported to accelerate the AgCl fragmentation and reduction. Based on the fact that LB broth is rich in yeast extract and peptone, which contains Ag-bound histidine and electron donor tyrosine too, we propose that yeast extract and peptone would play a fundamental role, involved first the formation of $[Ag^+]$-biomolecule monomers that further nucleate into AgCl clusters upon reaction with Cl^- ions. The AgCl nuclei might grow fast into well-dispersed ~ 50 nm colloids instead of micro-sized particles owing to the stabilization of biomoleucles (Scheme 1B). When solar light irradiates, the adsorbed molecules like peptide or DNA might facilitate the cleavage of AgCl particles due to high energy UV exposure; at the same time, AgCl is excited to generate electrons at the conduction band and then these electrons react with $[Ag^+]$ to form Ag NPs across the surface. The Ag NPs are able to absorb visible light and drive a collective and coherent oscillation of the electrons with the incident photons at the surface of NPs due to the localized surface plasmon resonance (LSPR). The decays of LSPR or the electron-phonon relaxation is generally coupled with the vibrations of the Ag and AgCl lattices and heating of the surrounding local environment. An extremely high transient temperature of the irradiation location is beneficial to functional Ag@AgCl synthesis.[31, 48] As shown in Scheme 1B, because of the heterogeneous size distribution associated with the random particle rupture, Ostwald ripening process is likely to be linked with the growth of Ag@AgCl in the following stage. The localized heating effect can enhance the rates of dissolution of smaller AgCl nanoparticles, due to their high surface area/energy and high density of surface defect. The super saturation of Cl^- and Ag^+ surrounding the larger particles would re-precipitate on the particle and help them resume to original AgCl particle size. Therefore, DLS measurements of the particles obtained before and after 5 min light irradiation remain constantly. The zeta potential of 40Ag LB5m samples is –30 mV. The negative surface charge is due to the termination of AgCl crystals by chlorine ions.[6, 40] Additionally, the adsorbed biological molecules like peptide or DNA might contribute to

the negative charge which is beneficial to separate the photon-generated carrier pairs.[41]

Photocatalytic mechanism studies on 40AgLB5m samples

Practically, solar light is the most economical energy source for the performance of the photocatalysts. Our sun simulator provides a spectral range from 300 nm up to 1100 nm, which can be used to compare catalysts responsive to UV or visible light wavelengths fairly. MB was firstly chosen to evaluate the degradation activity of the samples. As illustrated in Figure 5A, negligible MB degradation was observed in the absence of any catalyst under solar light illumination. Only 45% MB was degraded by 10AgLB5m within 15 min. By increasing the [Ag^+], the photoactivity of the particles greatly improves until reaches 40 mM. With this sample, MB was almost degraded within 10 min. Further increasing [Ag^+] to 80 mM leads to a reduced performance due to a lower light absorption as compared to 40AgLB5m sample. Figure 5B indicates that the removal efficiency of 90% methyl orange (MO) was obtained after 30 min reaction.

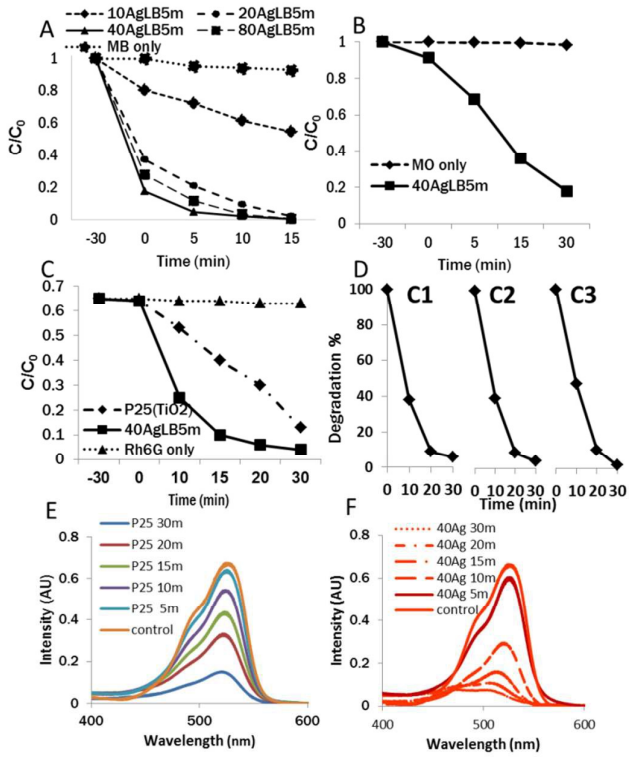

Fig. 5 The degradation curves of MB (A), MO (B) and Rh6G (C) solution over studied photocatalysts, (D) three cycling degradation curves of MO over 40AgLB5m under simulated solar light irradiation, and (E, F) UV-vis spectra changes of 15 mL Rh6G (10 ppm) in the presence of 7 mg of P25 and 40Ag5mLB5m under various solar light irradiation times.

Based on these results, 40AgLB5m was tested further on Rh6G decomposition and recyclability. For comparison, photoactivity of commercial P25 (TiO_2, Degussa Co. Ltd.) was measured under the same experimental conditions (Figure 5C). Interestingly, Ag@AgCl nanocomposite exhibited much better performance than P25. To evaluate the photostability of the catalysts, three successive cyclic Rh6G degradation tests under solar light were carried out, and it is found that 40AgLB5m remains high efficiency after three recycles (Figure 5D).

The Rh6G dye has an absorption maximum at λ_{max} = 524 nm. Time-dependent UV-vis spectra of Rh6G over P25 and 40AgLB5m catalysts clearly indicate their degradation mechanisms are different (Figure 5E and 5F). Blue-shifted peaks were observed only in the presence of 40AgLB5m and suggest that Rh6G molecules were decomposed through the loss of one or more ethyl groups.[42]

According to the literature, free radicals (e.g. superoxide anion ($\bullet O_2^-$), hydroxyl radicals ($\bullet$OH)), active chlorine (Cl^0) and photogenerated holes (h^+) are powerful species in photodegrading organic pollutants.[40, 43] To investigate the photocatalytic mechanism of 40AgLB5m, the PL technique with terephthalic acid (TA) as a probe molecule was employed to investigate the reactive oxygen species generated. Figure 6A shows the plots of fluorescence intensity versus solar light irradiation time for TA in the presence of 40AgLB5m. A characteristic fluorescence peak at ~ 426 nm indicates the production of $\bullet$OH radicals. A gradual enhancement of PL intensity was observed by prolonging the irradiation time. An ESR spin-trap technique, in the presence of 5,5-dimethyl-1-pyrroline N-oxide (DMPO) was further employed to probe the generation of other radicals. The ESR spectra, as shown in Figure 6B, prove the presence of two reactive oxygen species, with superoxide radicals ($\bullet O_2^-$) as the predominant species in the reaction system, which is in agreement with previous studies.[44]

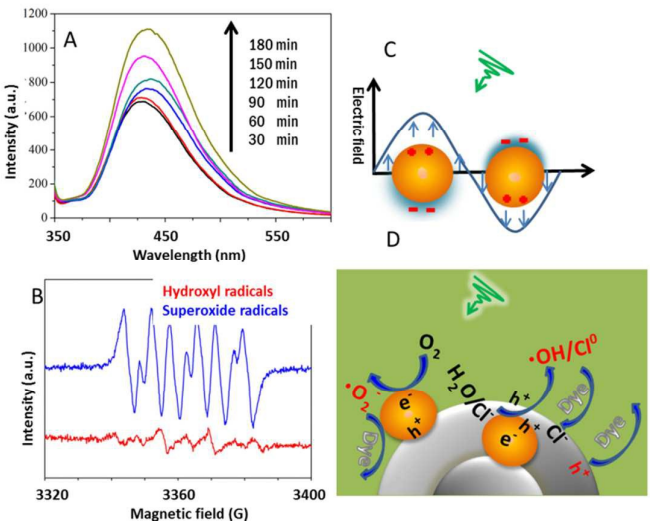

Fig. 6 (A) PL spectral changes versus solar light irradiation time of 40AgLB5m sample in terephthalic acid solution, (B) representative DMPO spin-trapping ESR signals of hydroxyl radicals and superoxide radicals, (C) Ag NPs surface plasmon resonance, and (D) Schematic diagram showing the possible mechanism for the photocatalytic degradation of dyes over the Ag@AgCl nanocomposites.

On the basis of the above results, the enhanced catalytic rates and excellent stability of 40AgLB5m can be explained in the following aspects. Firstly, the high performance of Ag@AgCl nanohybrids have been well documented in numerous studies and often attributed to the extended Ag SPR absorption in visible light region.[45] It is accepted that photon-excited electron and hole pair in Ag NPs could be sufficiently separated by the enhanced local electromagnetic field (Figure 6C).[14] The electron moving to the surface of the attached Ag NPs could react with the dissolved oxygen to form superoxide ions ($\bullet O_2^-$) for organic pollutants decomposition. Secondly, the encapsulated Ag NPs inside the AgCl matrix offer a unique configuration that is beneficial to better light utilization. The SPR properties depend on the size, shape and amount of the Ag NPS. A recent investigation revealed that NPs penetration depth, or the surface area of the Ag NPs in contact with the AgCl substrate, also influenced light absorption.[26] Based on classical electrodynamic calculations, it was found the Ag NPs embedding was more effective than the size in extending the absorption range of the visible light. When the Ag sphere was completely enclosed by the AgCl substrate, the dipole plasmon resonance induced the highest E-field enhancement, the nanocomposites response to wider range of light thereby producing more electrons and holes. Moreover, when Ag NPs were embedded inside the AgCl, electron would be more likely confined in the core of Ag NPs and the accumulated charges could be slowly released through diffusion across the Schottky junction.[46] This will allow the photo-generated holes have long life time to be transferred to AgCl surface driven by the negative AgCl surface charge, which may oxidize dye directly, may react with surface-bound H_2O or OH^- to produce the hydroxyl radical, or lead to the oxidation of Cl^- to Cl^0 and the subsequent dye degradation.[4, 16, 47-48] The enrichment of photo-excited electrons away from the AgCl surface also prevents photolysis of AgCl to Ag nanoclusters, thus renders the stability of Ag@AgCl. Thirdly, Ma and co-workers further experimentally proved that photo reduced Ag@AgCl possessed higher catalytic performance compared to chemical reduced Ag@AgCl, mainly due to a large amount of bulk defects.[26] In agreement with their discoveries, we believe that during solar light irradiation, bulk defects in 40AgLB5m samples could also be induced considering the large penetration depth of UV light.

Although more efforts are required to reveal the detailed Ag@AgCl formation and photocatalytic mechanisms, the relevant reactions can be listed as follows:

$$AgCl \xrightarrow{h\nu} e_{CB}^- + h_{VB}^+ \quad (2)$$

$$Ag^+ + e^- \xrightarrow{h\nu} Ag^0 \quad (3)$$

$$Ag@AgCl \rightarrow h^+ + e^- \quad (4)$$

$$Ag^0 (e^-) + O_2 \rightarrow \bullet O_2^- \quad (5)$$

$$AgCl\ (h^+) + H_2O/OH^- \rightarrow \bullet OH + H^+ \quad (6)$$

$$\bullet O_2^-, \bullet OH, h^+ + dyes \rightarrow CO_2 + H_2O \quad (7)$$

Experimental

Reagents and Materials

All of the chemicals were analytical grade and used as received without further purification. $AgNO_3$ (> 99%), ammonium hydroxide solution (NH_4OH, 28.0% NH_3 in water) and concentrated HNO_3 (70.4%) were purchased from Sigma-Aldrich. Nutrient broth (NB), tryptic soy broth (TSB), yeast mold broth (YMB), yeast extract (YE) and peptone in powder form were purchased from BD Company. Lysogeny broth (Miller) powder was purchased from Novagen Company. The aqueous broth was prepared by suspending broth powder in 1 L deionized (DI) water followed by autoclave at 121 °C for 15 min. Microbial contamination will not be an issue in the subsequent particle synthesis as the added $AgNO_3$ solutions ($[Ag^+] \geq 1$ mM) will effectively inhibit the growth of various microorganisms.

Synthesis of Ag@AgCl nanoparticles

Silver nitrate was dissolved in DI water to get a 160 mM stock solution. In a typical procedure of AgCl nanoparticle preparation, 10 mL $AgNO_3$ solution was added to 10 mL broth to get final $[Ag^+]$ concentrations from 1.0 to 80 mM. The mixture was then magnetically stirred under a solar simulator, 550 W Xenon lamp (ABET Technologies, Model 11016A Sun 3000), from 30 sec to 60 min. For comparison, control samples were prepared by direct mixing of $AgNO_3$ with NaCl, yeast extract or peptone solution followed by solar light irradiation. All nanoparticles were collected after centrifugation at 7000 rpm for 30 min. The precipitate was washed by water and dried in an oven at 60 °C. Small-scale (100 mL) experiments were carried out to obtain 40AgLB5m samples and there is no obvious difference between the final products. The larger-scale production may require optimization in sunlight exposure time.

Structural characterization of Ag@AgCl nanoparticles

The course of the colloids formation was monitored by a JASCO V-670 UV-Vis/NIR spectrophotometer. UV-vis diffuse reflectance spectra were recorded using $BaSO_4$ as a reference. The particle size and polydispersity were characterized by dynamic light scattering (DLS) using a Nano-ZS90 analyser (Malvern). X-ray diffraction analysis was performed on a Bruker D8 Advance X-ray Diffractometer with Cu Kα (λ = 1.54 Å) radiation. The diffracted intensities were recorded from 20° to 85° at 2θ angles. The morphologies of catalyst structures were investigated by a field-emission scanning electron microscope (Zeiss Neon 40EsB FIBSEM). For transmission electron microscopy (TEM), a drop of solution was placed on carbon-coated copper grids and air dried. TEM images, high-resolution transmission electron microscopic (HRTEM) images and the selected area electron diffraction (SAED) patterns were obtained on a JEOL-2010 microscope operated at accelerating voltage of 200 kV. X-ray photoelectron spectra (XPS) data were recorded using a Thermo ESCALAB 250XI electron spectrometer. All of the binding energies were calibrated using the contaminant carbon (C 1 s) at 284.6 eV as a reference. The electron spin resonance (ESR) signals of the radicals trapped by 5, 5-dimethyl-1-pyrroline N-oxide (DMPO) were detected at ambient temperature with a Bruker (E500) spectrometer. The irradiation source was a Quanta-Ray Nd:YAG pulsed laser system (k = 532 nm, 10 Hz). The settings

for the ESR spectrometer were as follows: center field = 3,510 G; sweep width = 200 G; microwave frequency = 9.85 GHz; modulation frequency = 100 kHz; and power = 20 mW. The photoluminescence (PL) characteristics were probed using a Hitachi F-4500 fluorescence spectrophotometer.

Photocatalytic activity of the Ag@AgCl nanoparticles Methylene blue (MB), methyl orange (MO) and Rhodamine 6G (Rh6G) aqueous solutions were prepared as the target organic pollutants to test the solar light-driven photocatalytic activities of the particles. The same 500 W Xenon lamp was used as the light source. In a typical phtotcatalytic reaction, the particle dispersion prepared after solar light illumination was centrifuged and the precipitate (~ 7 mg) was re-dispersed in 2.5 mL DI water and mixed with 10 mL dye solution (12.5 mg/L). The mixture was kept in dark for 30 min to achieve an equilibrium adsorption before light irradiation. Aliquots of the dispersion were taken out from the reaction system and centrifuged at 7000 rpm for 3 min before measuring absorption spectrum in the range of 400 to 750 nm.

Conclusions

Here we report a facile synthetic protocol for producing small plasmonic Ag@AgCl catalyst in microbe-free LB broth under mild conditions. The broth ingredients such as peptone, yeast extract and sodium chloride provide an ideal environment for the formation of Ag NP embedded AgCl nanohybrid with uniform size distribution. The photocatalytic results showed that the as-prepared samples possess high capability in organic dye degradation. The present study can open a new opportunity for the development of more advanced Ag@AgX-based ternary photocatalysts, such as Ag/AgCl@helical chiral TiO_2 to address energy conversion, green chemistry, and meet the environmental demands for the future, which is currently capturing the attention of worldwide researchers.[49-50]

Acknowledgements

L. Liu is supported by the Department of Chemical Engineering, Curtin University. This work was partially supported by the Australian Research Council (DP110104599 & DP150103026). The authors acknowledge the use of Curtin University's Microscopy & Microanalysis Facility, whose instrumentation has been partially funded by the University, State and Commonwealth Governments. The authors also acknowledge the provision of research facilities and the scientific and technical assistance of the staff of CHIRI Biosciences Research Precinct core facility, Curtin University. The authors are appreciating the great supports from Drs. X. Wang, G. Zhou, A. Chan, X. Hua and A. Werner.

Notes and references

‡ Z. Shen and B. Liu contributed equally.

1. W. L. Liu, F. C. Lin, Y. C. Yang, C. H. Huang, S. Gwo, M. H. Huang and J. S. Huang, *Nanoscale*, 2013, **5**, 7953-7962.
2. J. Manna, S. Goswami, N. Shilpa, N. Sahu and R. K. Rana, *ACS Appl. Mater. Interfaces*, 2015, **7**, 8076-8082.
3. Z. F. Shen, P. Liang, S. B. Wang, L. H. Liu and S. M. Liu, *ACS Sustain. Chem. Eng.*, 2015, **3**, 1010-1016.
4. P. Wang, B. B. Huang, Y. Dai and M. H. Whangbo, *Phys. Chem. Chem. Phys.*, 2012, **14**, 9813-9825.
5. M. C. Long and W. M. Cai, *Nanoscale*, 2014, **6**, 7730-7742.
6. P. Wang, B. B. Huang, X. Y. Qin, X. Y. Zhang, Y. Dai, J. Y. Wei and M. H. Whangbo, *Angew. Chem. Int. Ed.*, 2008, **47**, 7931-7933.
7. H. Y. Li, T. S. Wu, B. Cai, W. G. Ma, Y. J. Sun, S. Y. Gan, D. X. Han and L. Niu, *Appl. Catal. B Environ.*, 2015, **164**, 344-351.
8. H. X. Shi, G. Y. Li, H. W. Sun, T. C. An, H. J. Zhao and P. K. Wong, *Appl. Catal. B Environ.*, 2014, **158**, 301-307.
9. L. H. Dong, D. D. Liang and R. C. Gong, *Eur. J. Inorg. Chem.*, 2012, 3200-3208.
10. C. H. An, J. Z. Wang, W. Jiang, M. Y. Zhang, X. J. Ming, S. T. Wang and Q. H. Zhang, *Nanoscale*, 2012, **4**, 5646-5650.
11. Y. P. Bi and J. H. Ye, *Chem. Commun.*, 2009, 6551-6553.
12. L. Han, P. Wang, C. Z. Zhu, Y. M. Zhai and S. J. Dong, *Nanoscale*, 2011, **3**, 2931-2935.
13. D. L. Chen, S. H. Yoo, Q. S. Huang, G. Ali and S. O. Cho, *Chem. Eur. J.*, 2012, **18**, 5192-5200.
14. Y. X. Tang, Z. L. Jiang, G. C. Xing, A. R. Li, P. D. Kanhere, Y. Y. Zhang, T. C. Sum, S. Z. Li, X. D. Chen, Z. L. Dong and Z. Chen, *Adv. Funct. Mater.*, 2013, **23**, 2932-2940.
15. C. C. Han, L. Ge, C. F. Chen, Y. J. Li, Z. Zhao, X. L. Xiao, Z. L. Li and J. L. Zhang, *J. Mater. Chem. A*, 2014, **2**, 12594-12600.
16. Z. K. Xu, L. Han, P. Hu and S. J. Dong, *Catal. Sci. Tech.*, 2014, **4**, 3615-3619.
17. J. H. Kou and R. S. Varma, *Chemsuschem*, 2012, **5**, 2435-2441.
18. A. A. Kulkarni and B. M. Bhanage, *ACS Sustain. Chem. Eng.*, 2014, **2**, 1007-1013.
19. C. C. Jiang, Z. Y. Guo, Y. Zhu, H. Liu, M. X. Wan and L. Jiang, *Chemsuschem*, 2015, **8**, 158-163.
20. C. Liu, D. Yang, Y. G. Wang, J. F. Shi and Z. Y. Jiang, *J. Nanopart. Res.*, 2012, **14**, 1084-1095.
21. X. Zhao, J. Zhang, B. Wang, A. Zada and M. Humayun, *Materials*, 2015, **8**, 2043-2053.
22. J. A. Rollin, T. K. Tam and Y. H. P. Zhang, *Green Chem.*, 2013, **15**, 1708-1719.
23. L. H. Liu, Z. P. Shao, H. M. Ang, M. O. Tade and S. M. Liu, *RSC Adv.*, 2014, **4**, 14564-14568.
24. L. H. Liu, T. T. Liu, M. Tade, S. B. Wang, X. Y. Li and S. M. Liu, *Enzyme Microb. Technol.*, 2014, **67**, 53-58.
25. S. Kracht, M. Messerer, M. Lang, S. Eckhardt, M. Lauz, B. Grobety, K. M. Fromm and B. Giese, *Angew. Chem. Int. Ed.*, 2015, **54**, 2912-2916.
26. X. C. Ma, Y. Dai, L. Yu, Z. Z. Lou, B. B. Huang and M. H. Whangbo, *J. Phys. Chem. C*, 2014, **118**, 12133-12140.
27. M. S. Zhu, P. L. Chen, W. H. Ma, B. Lei and M. H. Liu, *ACS Appl. Mater. Interfaces*, 2012, **4**, 6386-6392.
28. M. S. Zhu, P. L. Chen and M. H. Liu, *Langmuir*, 2013, **29**, 9259-9268.
29. A. E. Morales, E. S. Mora and U. Pal, *Revista Mexicana de Fisica S*, 2007, **53**, 18-22.
30. J. Song, J. Roh, I. Lee and J. Jang, *Dalton Trans.*, 2013, **42**, 13897-13904.
31. S. Peng and Y. G. Sun, *J. Mater. Chem.*, 2011, **21**, 11644-11650.

32. P. Barone, F. Stranges, M. Barberio, D. Renzelli, A. Bonanno and F. Xu, *J. Chem.*, 2014, 589707 (6 pages).
33. L. Q. Ye, J. Y. Liu, C. Q. Gong, L. H. Tian, T. Y. Peng and L. Zan, *ACS Catal.*, 2012, **2**, 1677-1683.
34. S. Behrens, J. Wu, W. Habicht and E. Unger, *Chem. Mater.*, 2004, **16**, 3085-3090.
35. Z. D. Huang, M. Wen, D. D. Wu and Q. S. Wu, *RSC Adv.*, 2015, **5**, 12261-12267.
36. Y. Liu, R. G. Jordan and S. L. Qiu, *Phys. Rev. B*, 1994, **49**, 4478-4484.
37. B. Chai, X. Wang, S. Cheng, H. Zhou and F. Zhang, *Ceram. Int.*, 2014, **40**, 429-435.
38. Y. Zhang, M. Ding, L. Ma, T. Wang and X. Li, *RSC Adv.*, 2015, **5**, 58727-58733.
39. G. Wang, T. Nishio, M. Sato, A. Ishikawa, K. Nambara, K. Nagakawa, Y. Matsuo, K. Niikura and K. Ijiro, *Chem. Commun.*, 2011, **47**, 9426-9428.
40. Z. Y. Lin, J. Xiao, J. H. Yan, P. Liu, L. H. Li and G. W. Yang, *J. Mater. Chem. A*, 2015, **3**, 7649-7658.
41. G. Q. Wang, H. Mitomo, Y. Matsuo, N. Shimamoto, K. Niikura and K. Ijiro, *J. Mater. Chem. B*, 2013, **1**, 5899-5907.
42. W. T. Liu, D. L. Chen, S. H. Yoo and S. O. Cho, *Nanotechnology*, 2013, **24**, 405706 (7 pages).
43. Y. L. Ren, Q. D. Zhao, X. Y. Li, W. Xiong, M. Tade and L. H. Liu, *J. Nanopart. Res.*, 2014, **16**, 2532(8 pages).
44. X. J. Bai, L. Wang, R. L. Zong and Y. F. Zhu, *J. Phys. Chem. C*, 2013, **117**, 9952-9961.
45. H. Xu, H. M. Li, J. X. Xia, S. Yin, Z. J. Luo, L. Liu and L. Xu, *ACS Appl. Mater. Interfaces*, 2011, **3**, 22-29.
46. X. M. Zhang, Y. L. Chen, R. S. Liu and D. P. Tsai, *Rep. Prog. Phys.*, 2013, **76**, 046401 (41 pages).
47. B. W. Ma, J. F. Guo, W. L. Dai and K. N. Fan, *Appl. Catal. B Environ.*, 2013, **130**, 257-263.
48. J. Jiang and L. Z. Zhang, *Chem-Eur J*, 2011, **17**, 3710-3717.
49. D. Wang, Y. Li, G. L. Pum, C. Wang, P. Wang, W. Zhang and Q. Wang, *Chem. Commun.,* 2013, **49**, 10367-10369.
50. C. Zhang, Y. Li, D. Wang, W. Zhang, Q. Wang, Y. Wang and P. Wang, *Environ. Sci. Pollut. Res.*, 2015, **22**, 10444–10451.

Sustainable synthesis of highly efficient sunlight-driven Ag embedded AgCl photocatalyst

Z. Shen[a, ‡], B. Liu[b, ‡], V. Pareek[a], S. Wang[a], X. Li[b], L. Liu[a,] and S. Liu[a]*

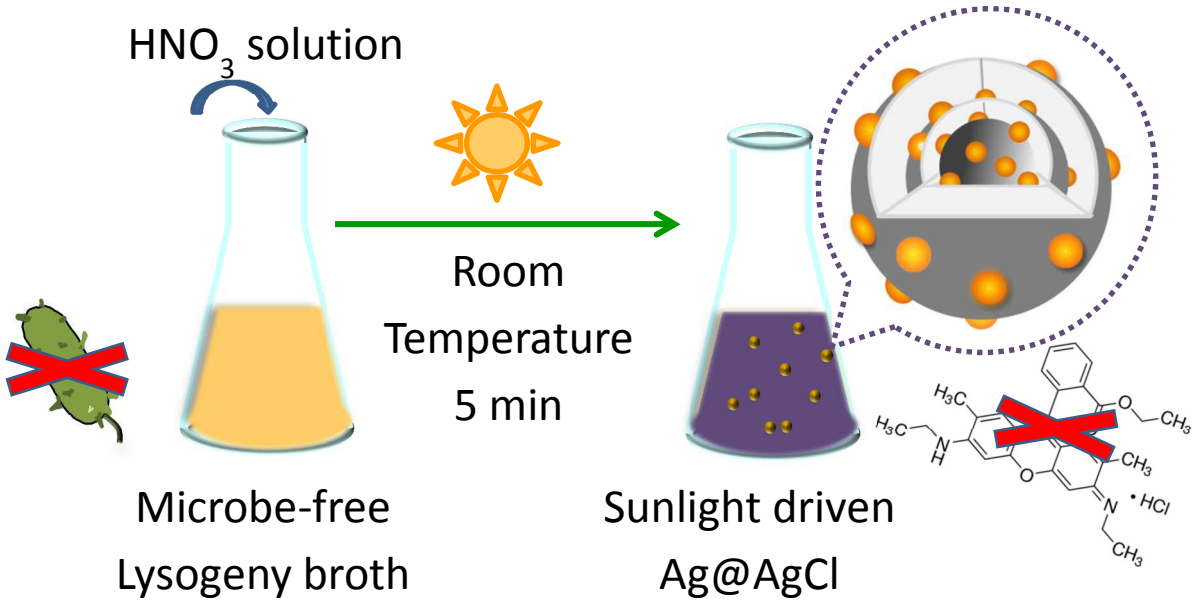

Microbe-free broth synthesis was performed under solar light gave Ag nanoparticle embedded AgCl in 5 minutes with superior performance than P25 for organic pollutant degradation.